Provided for non-commercial research and education use.
Not for reproduction, distribution or commercial use.

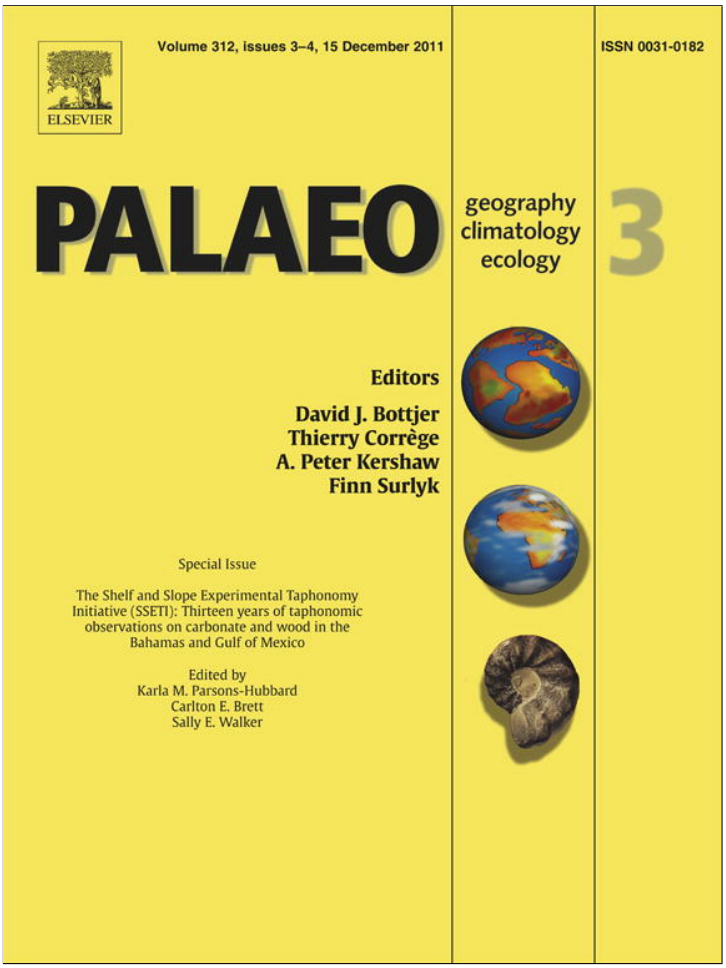

This article appeared in a journal published by Elsevier. The attached copy is furnished to the author for internal non-commercial research and education use, including for instruction at the authors institution and sharing with colleagues.

Other uses, including reproduction and distribution, or selling or licensing copies, or posting to personal, institutional or third party websites are prohibited.

In most cases authors are permitted to post their version of the article (e.g. in Word or Tex form) to their personal website or institutional repository. Authors requiring further information regarding Elsevier's archiving and manuscript policies are encouraged to visit:

http://www.elsevier.com/copyright

Author's personal copy

Palaeogeography, Palaeoclimatology, Palaeoecology 312 (2011) 265–277

Contents lists available at ScienceDirect

Palaeogeography, Palaeoclimatology, Palaeoecology

journal homepage: www.elsevier.com/locate/palaeo

Geochemical environments of continental shelf-upper slope sediments in the northern Gulf of Mexico

Xinping Hu [a], Wei-Jun Cai [a,*], Yongchen Wang [a], Xianghui Guo [a,b,1], Shangde Luo [c]

[a] Department of Marine Sciences, University of Georgia, Athens, GA 30602, USA
[b] State Key Laboratory of Marine Environmental Science, Xiamen University, Xiamen, Fujian, China
[c] Department of Earth Sciences, National Chung-Kung University, Tainan 701, Taiwan

ARTICLE INFO

Article history:
Received 7 June 2010
Received in revised form 23 March 2011
Accepted 13 April 2011
Available online 28 April 2011

Keywords:
Carbonate dissolution
Taphonomy
Geochemistry
Sediments
Gulf of Mexico

ABSTRACT

Geochemical environments were characterized for 14 sites along the northern Gulf of Mexico continental shelf and upper slope, in an effort to examine the relationship between sediment geochemistry and carbonate shell taphonomy in a long-term study—Shelf and Slope Experimental Taphonomy Initiative (SSETI). Three groups of environments of preservation (seep, near-seep, and shelf-and-slope) were identified based on their geochemical characteristics (i.e., oxygen uptake rate and penetration depth, pore-water saturation states, and carbonate dissolution fluxes). Diffusive oxygen uptake rate increased in the order of shelf-and-slope, near-seep, and seep, although carbonate dissolution flux did not show significant correlation with O_2 flux, presumably due to non-diffusive behavior at some sites. Using pore-water saturation indices with respect to aragonite and calcite and sedimentation rates, we defined a semi-quantitative parameter, carbonate dissolution index (CDI), to predict carbonate preservation potential during the taphonomic processes. Our limited database suggests that both the seep and the shelf-and-slope sediments may have higher carbonate preservation potential than the near-seep sediments.

© 2011 Elsevier B.V. All rights reserved.

1. Introduction

Postmortem skeletal remains of calcareous organisms undergo taphonomic changes (Parsons et al., 1997; Powell et al., 2008). These changes are generally categorized into two types, i.e., physical and chemical alterations. Physical processes include shell breakage and abrasion (Smith and Nelson, 2003); whereas chemical processes mostly involve dissolution and precipitation, as well as discoloration (Smith and Nelson, 2003; Powell et al., 2008). For chemical alterations, sediment geochemical characteristics, i.e., redox and carbonate saturation states are responsible for the extent of carbonate shell preservation and alteration (Sanders, 2003; Smith and Nelson, 2003; Best et al., 2007). In particular, it has been recognized that saturation states with respect to shell carbonate minerals of the aqueous medium, in which the shells are buried, exert direct control on shell dissolution, a major part of shell destruction (e.g., Sanders, 2003). In a sedimentary environment, pore-water saturation states are controlled by a host of geochemical parameters, including types of diagenetic reactions (Boudreau and Canfield, 1993), openness of the sediment system (i.e., presence of bioturbation and bioirrigation) (Ku et al., 1999), and the presence of inhibiting factors (such as iron that prevent recycling of reduced sulfur species, the latter process produces acid) (Kidwell et al., 2005; Perry and Taylor, 2006; Best et al., 2007). On the other hand, shell dissolution also depends on the characteristics of the shell materials, including carbonate mineralogy (being either calcitic or aragonitic) and associated organic matrices, and surface-to-volume ratio (e.g., Smith and Nelson, 2003). However, among all these different parameters, a quantitative linkage between pore-water carbonate saturation state and shell preservation/loss is still lacking, despite the fact that it has been realized that pore-water undersaturation is the driving force for carbonate shell dissolution (Alexandersson, 1975, 1978; Aller, 1982; Green et al., 1992, 1993).

In an attempt to investigate the relationship between sediment geochemistry and carbonate shell taphonomy, we joined two SSETI (Shelf and Slope Experimental Taphonomy Initiative) cruises to the northern Gulf of Mexico. The SSETI program is a long-term study that was conceived to examine taphonomic rates of skeletal materials (mainly carbonate) in a series of environments of preservation (EOPs) (Parsons et al., 1997). In 1993, the SSETI team deployed experiments (carbonate shell assemblages and wood materials) along the continental shelf and upper slope of the Gulf of Mexico (Fig. 1). In August 2001 and August 2006, two extractions of these early deployed experiments were carried out and a host of accompanying sediment cores near the

* Corresponding author. Tel.: +1 706 542 1285; fax: +1 706 542 5888.
E-mail address: wcai@uga.edu (W.-J. Cai).
[1] Current address: Research Center for Environmental Changes, Academia Sinica, 128 Sec. 2, Academia Rd., Nankang, Taipei, Taiwan.

0031-0182/$ – see front matter © 2011 Elsevier B.V. All rights reserved.
doi:10.1016/j.palaeo.2011.04.010

Author's personal copy

shell deployment sites were taken to study sediment geochemical properties. Our prior work (Cai et al., 2006) compared shell dissolution at a seep site and its surrounding areas and provided a geochemical interpretation for the existence of a taphonomically-active zone at this site, which is represented by a spatially limited low pH and under-saturation window associated with a highly compressed redox front in pore waters. In the present work, we will expand our site coverage of the northern Gulf of Mexico to include a variety of depositional environments along the continental shelf and upper slope, in order to explore a more generalized relationship between carbonate preservation and sediment geochemistry. To do this, we propose a new concept, carbonate dissolution index (CDI), and hypothesize that this parameter can be used to examine taphonomic activeness of sedimentary environments. Note our CDI is different from the shell dissolution index as reported in previous SSETI studies (Powell et al., 2002; Cai et al., 2006), where the non-parametric dissolution index values referred to the extent of shell dissolution.

2. Materials and methods

2.1. Site descriptions

Sediments and pore waters were collected at 14 sites along the continental shelf and upper slope of the northern Gulf of Mexico (Table 1 and Fig. 1) during our August–September, 2006 cruise on board R/V *Seward Johnson* and submersible *Johnson Sea-Link I*. Sediments at these locations are mainly of terrigenous origin (Powell et al., this issue; also see Cai et al., 2006).

2.2. Sample collection and processing

Push cores were collected using 30 cm-long butyl core tubes (i.d. = 8 cm) equipped with one-way check valves at the top of these core tubes. This design facilitates the entrapped water in the upper core tube to escape through the check valve as a core tube was slowly inserted into sediment. Four to five whole sediment cores with lengths ranging ~18–25 cm were collected at each site. Immediately upon the arrival of sediment cores on board, they were sealed at the bottom using rubber stoppers and then transferred to a shipboard cold room, which was maintained at near bottom water temperature (7–8 °C). Visual inspection of these cores did not observe carbonate crusts or macro-fauna. One intact core from each site was kept under in situ temperature in a circulating water bath for microelectrode profiling. Core sectioning was carried out using a hydraulic extruder (Joye et al., 2004; Cai et al., 2006). The depth intervals sampled were 0–1, 1–2, 2–3, 3–5, 5–7, 7–10, 10–14, and 14–17 cm. One sectioned core from each site was immediately preserved at −20 °C for solid phase carbon analysis, and all other sectioned core intervals were compressed under N_2 pressure within two hours of core recovery using the same gas-actuated Reeburgh-type core squeezers as described in Joye et al. (2004). Pore-water samples were received using 50-ml disposable plastic syringes, and then they were filtered through 0.45-μm nylon disk filters into appropriate storage vessels for further analyses. Total alkalinity (TAlk) and dissolved inorganic carbon (DIC) samples were preserved using saturated $HgCl_2$ solution (0.02 ml for every 5 ml of sample). Sulfate samples were acidified using concentrated HNO_3 (0.1 ml for every 0.5 ml of sample) to expel H_2S as sulfide reoxidation could produce sulfate during sample preservation (Joye, per. comm.). All pore-water samples were kept refrigerated at 4 °C in the dark until analysis.

2.3. Sediment organic carbon and carbonate concentrations

Frozen surface sediment samples were first thawed and dried at 60 °C overnight. Then they were pulverized using a stainless steel ball mill. Total carbon and organic carbon was determined using a Carlo Erba NA 1500 elemental analyzer (Analytical Chemistry Lab, UGA) on untreated and acidified samples, and 1 M HCl was used to remove carbonate. Sediment carbonate concentration was calculated using the difference between the total and organic carbon concentrations assuming $CaCO_3$ was the sole carbonate form. Relative uncertainties of total and organic carbon analysis were 2% and 5%, respectively.

2.4. Electrochemical and pore-water analysis

Within hours of core recovery, micro-profiling of pore-water oxygen and pH was carried out on the intact core from each site, using a commercial oxygen microelectrode (Unisense®, Denmark) and a home-made glass pH microelectrode (Cai and Reimers, 1993), respectively. The oxygen electrode was calibrated through a two-point calibration (e.g., Wang et al., 1999), using air-saturated seawater (100%) with known salinity and pore water at sediment depth where the electrode reached a minimum reading and presumably no dissolved oxygen was present (0%). A pH microelectrode and an Orion® Ross combination pH electrode were calibrated using the NBS pH buffers 4.00, 7.00, and 10.00 and then left together in the overlying water of the sediment core for 30 min to stabilize. The Ross electrode served as the reference to verify the stability of the microelectrode before and after the pH profiling. The small drift of the microelectrode was corrected by comparing the two values measured by both electrodes. After the microelectrode profiling for pH was complete, which was typically done in the upper few cm of a sediment core, the core tube was drilled at 1–2 cm intervals from the sediment–water interface downward and pore-water pH was measured by punching in an Orion® Ross mini-electrode (6-mm diameter). Both microelectrode and mini-electrode yielded consistent pH profiles. However, the former provides the needed high spatial resolution at the sediment–water interface (Cai et al., 2006). Microelectrode data reported here were averages of three repeated measurements in the same core.

Pore-water TAlk was determined by Gran titration. DIC was determined using an infrared CO_2 detector after acid extraction (Cai and Wang, 1998). Accuracy of TAlk and DIC analyses was assured by using a certified reference material (CRM) obtained from A. Dickson (Scripps Institute of Oceanography). Total halides were determined by $AgNO_3$ titration with potassium chromate/potassium dichromate as the end-point indicator (Grasshoff et al., 1999). This measurement will be referred to as chloride concentration because Br^- and I^- concentrations together rarely exceed 1 mM (less than 0.2% of chloride concentration) in both deep sea sediments (Gieskes and Mahn, 2007) and sediments that contain gas hydrates (e.g., Muramatsu et al., 2007). Sulfate concentration was determined using ion chromatography (IC) (Grasshoff et al., 1999). NaCl solution and IAPSO seawater were used as standards in $AgNO_3$ titration and IC analysis, respectively (Grasshoff et al., 1999). Calcium concentration was determined using EGTA titration (Grasshoff et al., 1999). EGTA titrant was standardized using standard solutions made from analytical $CaCO_3$ reagent following the procedures in Grasshoff et al. (1999). Uncertainties of pore-water analyses were: TA (±0.2%), DIC (±0.2%), Ca^{2+} (±0.2%), sulfate (±1%), and Cl^- (±0.2%).

In calculating carbonate saturation states, we took the microelectrode pH data and the DIC values interpolated from measured data at the depths where pH measurements were taken to calculate $[CO_3^{2-}]$ (e.g., Cai et al., 2006) at in situ temperature and pressure using the program CO2SYS (Lewis and Wallace, 1998). Carbonic acid dissociation constants were from Mehrbach et al. (1973) as refitted by Dickson and Millero (1987). Then ionic product ($[Ca^{2+}][CO_3^{2-}]$) was calculated using interpolated calcium concentration and calculated carbonate ion concentration. Carbonate saturation state was expressed as $\Omega = [Ca^{2+}][CO_3^{2-}]/K_{sp}'$. Calcite and aragonite stoichiometric dissolution constants (K_{sp}') were from Mucci (1983).

Author's personal copy

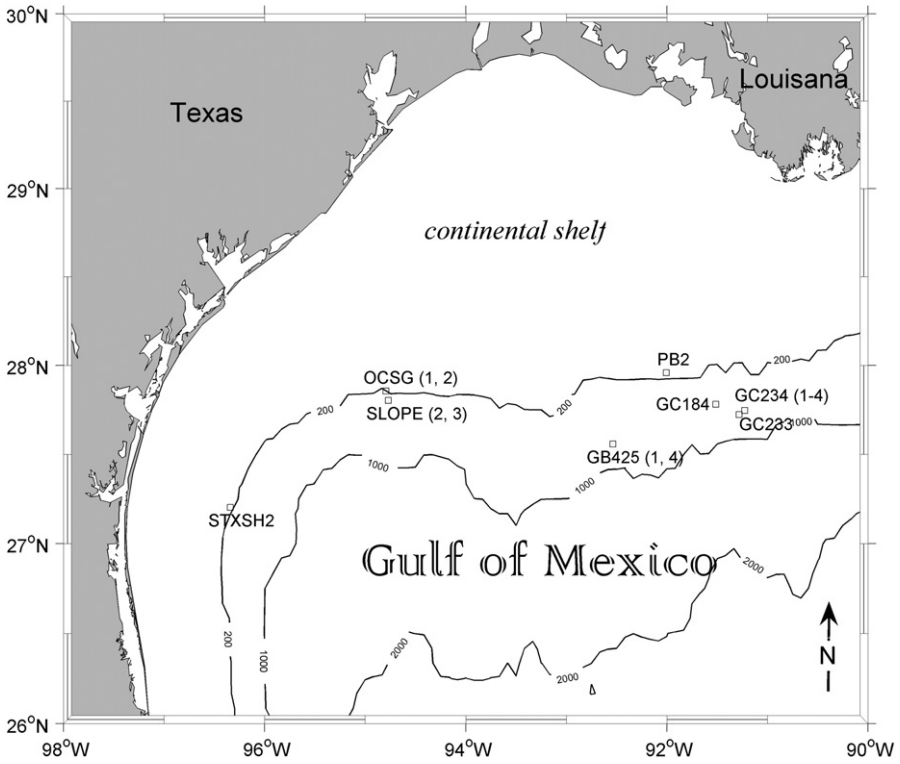

Fig. 1. The map of sampling locations in the northern Gulf of Mexico.

3. Results

Both sediment property (e.g., porosity) and pore-water geochemistry exhibited significant differences among all 14 sampled sites. These sites can be categorized into three major groups based on their locations and associated geochemical characteristics, i.e., seep sediments (directly affected by seep activities), including GB425-1, GC183, GC233, GC234-2; near-seep sediments (near petroleum seep locations but not directly affected by the seeps), including GC234-1, 3, 4; and the shelf-and-slope sediments, including SLOPE-2, 3, STXSH2, PB2, OCSG-1, 2.

3.1. Sediment porosity

Sediment porosity can be expressed as an exponential decay function of depth (Fig. 2, e.g., Boudreau, 1997):

$$\varphi = \varphi_{inf} + \left(\varphi_0 - \varphi_{inf}\right)e^{-az} \quad (1)$$

here φ is sediment porosity, subscripts *inf* and 0 represent infinite depth and sediment–water interface, a is a non-zero constant, z is depth. According to the curve fits, all seep sediments had significantly lower predicted φ_{inf} ($69.0 \pm 7.7\%$) compared to all other sites, whereas φ_{inf} at the near-seep and the shelf-and-slope sediments were not significantly different (i.e., $80.1 \pm 2.1\%$ vs. $82.1 \pm 2.9\%$).

3.2. Surface sediment organic carbon and carbonate concentrations

Except the shallowest site PB2, where the lowest organic carbon (0.7%) and the highest carbonate concentration (52.9%) were observed (Table 2), surface sediment organic carbon and carbonate concentrations from all other sites had ranges of 0.9–3.9% (in % weight of C) and 8.3–23.1% (in % weight of $CaCO_3$), respectively. These values are in agreement with the literature reported values for the sediments in the shelf and slope areas of the northern Gulf of Mexico (Gallaway et al., 1988; Morse and Beazley, 2008; Rowe and Kennicutt, 2009). Furthermore, the seep sites appeared to have higher but variable organic carbon

Table 1
Sampling locations and depths, bottom-water salinity and temperature, and general sediment descriptions.

Site	Location	Depth (m)	Salinity	Temp (°C)	Sediment description
GB425-4	92°32.39′W 27°37.48′N	570	34.9	7.4	Seep, gray to black, with patchy microbial mats
SLOPE-3	94°46.23′W 27°48.16′N	362	34.9	11.0	Brownish gray
STXSH2	96°20.51′W 27°12.20′N	181	36.1	16.3	Bioturbated, brown to gray, sandy
OCSG-2	94°47.57′W 27°51.36′N	180	35.9	14.6	Brown to gray, sandy
OCSG-1	94°47.62′W 27°51.36′N	180	36.0	15.4	Brown to gray, sandy
SLOPE-2	94°46.21′W 27°48.23′N	365	35.4	11.2	Brown to gray, sandy
GB425-1	92°32.30′W 27°33.59′N	571	34.9	7.4	Seep, brown to dark gray, abundant dead shells
PB2	92°00.27′W 27°57.51′N	116	36.6	22.0	Brown to gray, sandy
GC234-4	91°13.51′W 27°44.69′N	529	35.0	8.3	Brown to gray, fine mud
GC234-3	91°13.39′W 27°44.75′N	542	35.1	8.9	Brown to dark gray, sandy
GC234-2	91°13.61′W 27°44.75′N	532	35.0	8.2	Seep, bioturbated, gray to dark gray, oil present, fine mud
GC234-1	91°13.52′W 27°44.78′N	545	35.0	8.1	Brown to gray, fine mud
GC-184	91°30.70′W 27°46.80′N	544	35.0	8.0	Seep, brown to dark gray, bioturbated
GC-233	91°16.93′W 27°43.35′N	650	34.9	7.1	Seep, dark gray to black, fine mud

Author's personal copy

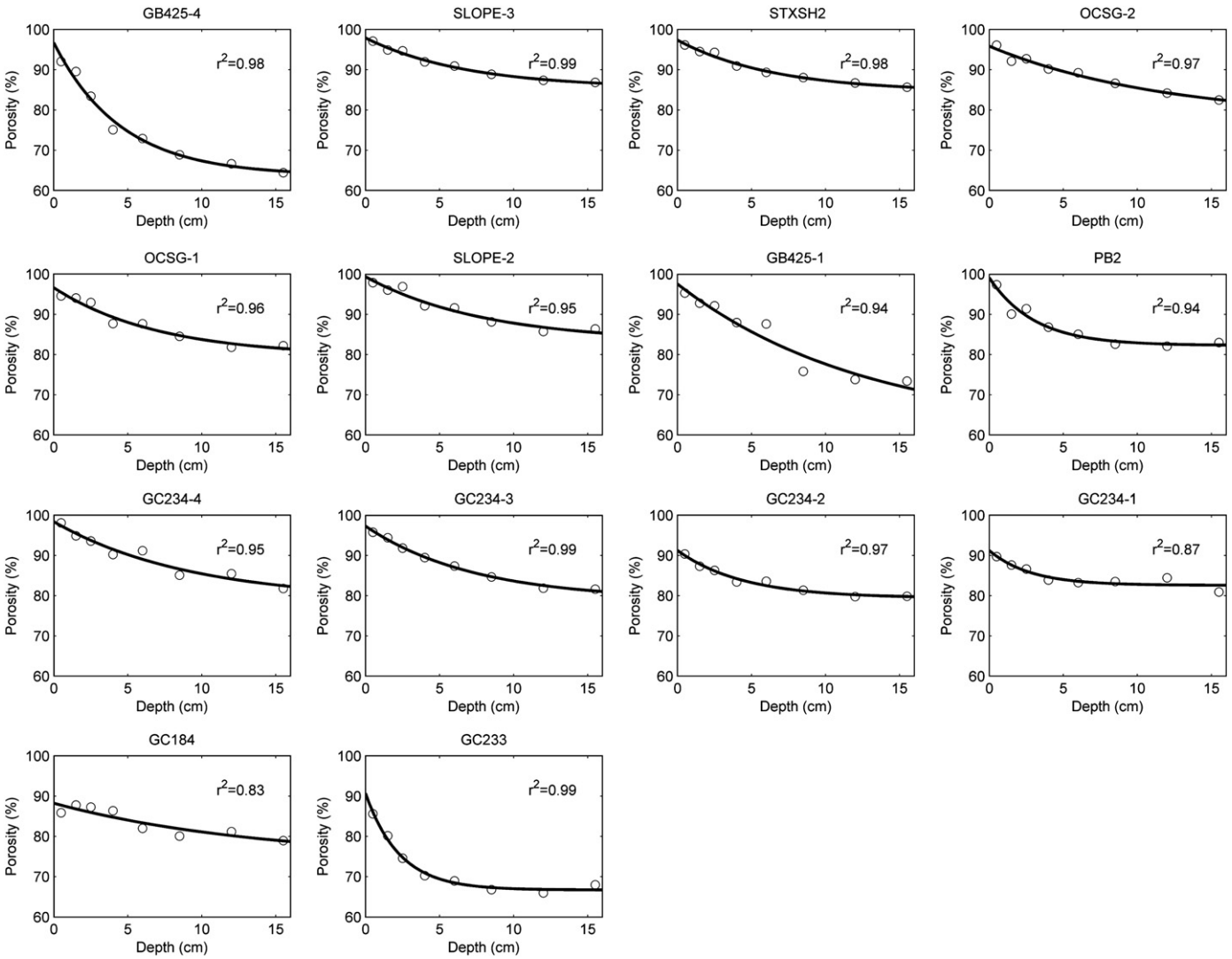

Fig. 2. Sediment porosity profiles. The curves are exponential fits of the data points.

concentrations and lower carbonate concentrations compared to the other sites, the latter were ~50% of those from both the near-seep and the shelf-and-slope sediments.

Table 2
Surface sediment organic carbon and carbonate concentrations.

Sediment type	Site ID	OC%	$CaCO_3$%
Seep	GB425-4	1.3	9.2
	GB425-1	1.4	8.3
	GC234-2[a]	3.9	8.5
	GC184	2.9	9.2
	GC233	0.9	17.0
	Average	2.1 ± 1.3	10.5 ± 3.7
Near-seep	GC234-4	1.3	20.1
	GC234-3	1.0	23.1
	GC234-1	1.0	19.0
	Average	1.1 ± 0.1	20.7 ± 2.2
Shelf-and-slope	SLOPE-3	1.4	17.8
	STXSH2	1.3	14.4
	OCSG-2	1.1	18.7
	OCSG-1	1.3	20.1
	SLOPE-2	1.5	15.7
	PB2	0.7	52.9
	Average	1.2 ± 0.3	23.3 ± 14.7

[a] Tubeworms were observed nearby.

3.3. General trends in pore-water geochemistry

3.3.1. Oxygen penetration depth and benthic fluxes

Distinct differences in oxygen penetration depths were observed at the sampling sites (Fig. 3). In the seep sediments, oxygen penetration depths were the shallowest (0.2–0.5 cm), the penetration depths in the near-seep sediments were greater (0.7–1.1 cm), and the shelf-and-slope sediments had the greatest oxygen penetration (1.5–2.0 cm). Using a second order polynomial curve fitting on collected pore-water O_2 profile (Cai and Sayles, 1996) and the extrapolated porosity (Section 3.1) at the sediment–water interface, we calculated diffusive flux of O_2 in these sediments (Table 3). The diffusion coefficient were calculated following Boudreau (1997) and corrected against sediment tortuosity using the equation $D_s = D_0/(1-\ln\varphi^2)$. Here D_0 is the diffusion coefficient in free solution. In addition, using the calcium concentration gradient between the bottom water and the topmost depth interval (i.e., 0–1 cm), we also calculated calcium diffusive fluxes using Fick's First Law (Berner, 1980) (Table 3).

3.3.2. Pore-water solute concentrations

Pore-water [Cl^-] exhibited various increases at these sites (Fig. 4a). The seep sites GB425-1 and GC233 had the highest [Cl^-] increase, i.e., at core bottom [Cl^-] were greater than 700 mmol kg^{-1} compared to the bottom-water concentration of ~550 mmol kg^{-1}.

Author's personal copy

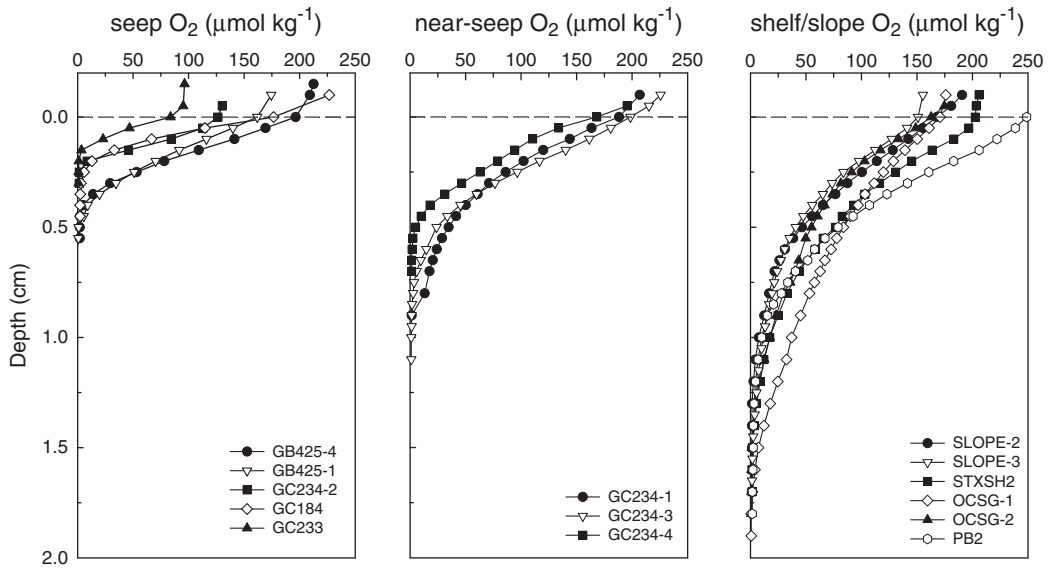

Fig. 3. Pore-water O_2 profiles. The dashed lines represent the sediment–water interface.

In comparison, shelf-and-slope sediments had only slight [Cl^-] changes except at the STXSH2 site, where a downcore increase in [Cl^-] (~50 mmol kg^{-1}) was observed. Changes in [Cl^-] often indicate a mixing between normal salinity seawater and high salinity brine water, the latter originated from the dissolution of the salt deposit in the continental slope area of the northern Gulf of Mexico and associated with petroleum seep activities (Joye et al., 2005). However, there was no observed seep activity at the STXSH2 site (E. Powell, pers. comm.).

The seep sediments also had the largest changes in other pore-water solute concentrations, as represented by elevated TAlk, DIC and depressed [SO_4^{2-}], which were especially evident at GB425-1 and GC233 (Fig. 4b–d). Pore-water profiles from these two sites have been attributed to physical mixing between the bottom seawater and the underlying brine that has high concentrations of metabolic products (DIC and TAlk) but low levels of sulfate, and the brine water is being advected from underneath the subsurface reaction front (Hu et al., 2010). In comparison, the other two seep sites (GC184 and GC234-2) appeared to be less influenced by brine activities. [Ca^{2+}] was usually higher in the pore waters than the bottom waters (Fig. 4e, top panel), although the calcium profiles at both GC233 and GC234-3 showed a downcore decreasing trend from below the sediment–water interface. In comparison, the near-seep sediments exhibited smaller changes in these pore-water solutes, and the shelf-and-slope sediments had the least changes. Furthermore, the [Ca^{2+}]:[Cl^-] ratio in the seep sediments showed slight increases within 2-cm below the sediment–water interface (note GC234-2 had a net increase throughout the sampled core). However, the depth ranges with elevated [Ca^{2+}]:[Cl^-] ratios in the near-seep and the shelf-and-slope sites were greater, i.e., 5–10 cm at the near-seep sites and entire sampled core at the shelf-and-slope sites, respectively (Fig. 4e, bottom panel).

3.3.3. pH and carbonate saturation state

Bottom water pH values ranged between 7.8 and 8.2 and all bottom waters were supersaturated with respect to both calcite and aragonite (Table 3 and Fig. 5). Both pH and carbonate saturation state

Table 3
Bottom water chemistry and calculated diffusive fluxes of dissolved species.

Sediment type	Site ID	$\Omega_{cal\text{-}BW}$	pH_{BW}	Ω_{min}	O_2 flux (mmol m^{-2} d^{-1})	Ca^{2+} flux (mmol m^{-2} d^{-1})
Seep	GB425-4	2.02	7.77	–	8.17	–
	GB425-1	2.00	7.75	0.79	6.20	8.20
	GC234-2[a]	2.12	7.78	0.83	6.50	3.28
	GC184	2.05	7.76	0.56	10.64	8.43
	GC233	2.05	7.76	0.44	7.08	8.84
	Average				7.72 ± 1.80	7.19 ± 2.62
Near-seep	GC234-4	2.06	7.77	0.39	5.76	4.83
	GC234-3	2.12	7.78	0.61	5.78	10.88
	GC234-1	2.10	7.77	0.49	4.27	4.33
	Average				5.27 ± 0.86	6.68 ± 3.56
Shelf-and-slope	SLOPE-3	2.51	7.84	0.73	3.77	5.89
	STXSH2	3.31	7.96	0.92	4.72	3.14
	OCSG-2	3.15	7.93	0.89	3.88	4.20
	OCSG-1	3.31	7.95	0.93	2.93	4.72
	SLOPE-2	2.38	7.82	0.58	4.12	7.74
	PB2	4.99	8.15	1.36	7.64	4.51
	Average				4.51 ± 1.64	5.04 ± 1.59

[a] Tubeworms were observed nearby.

Author's personal copy

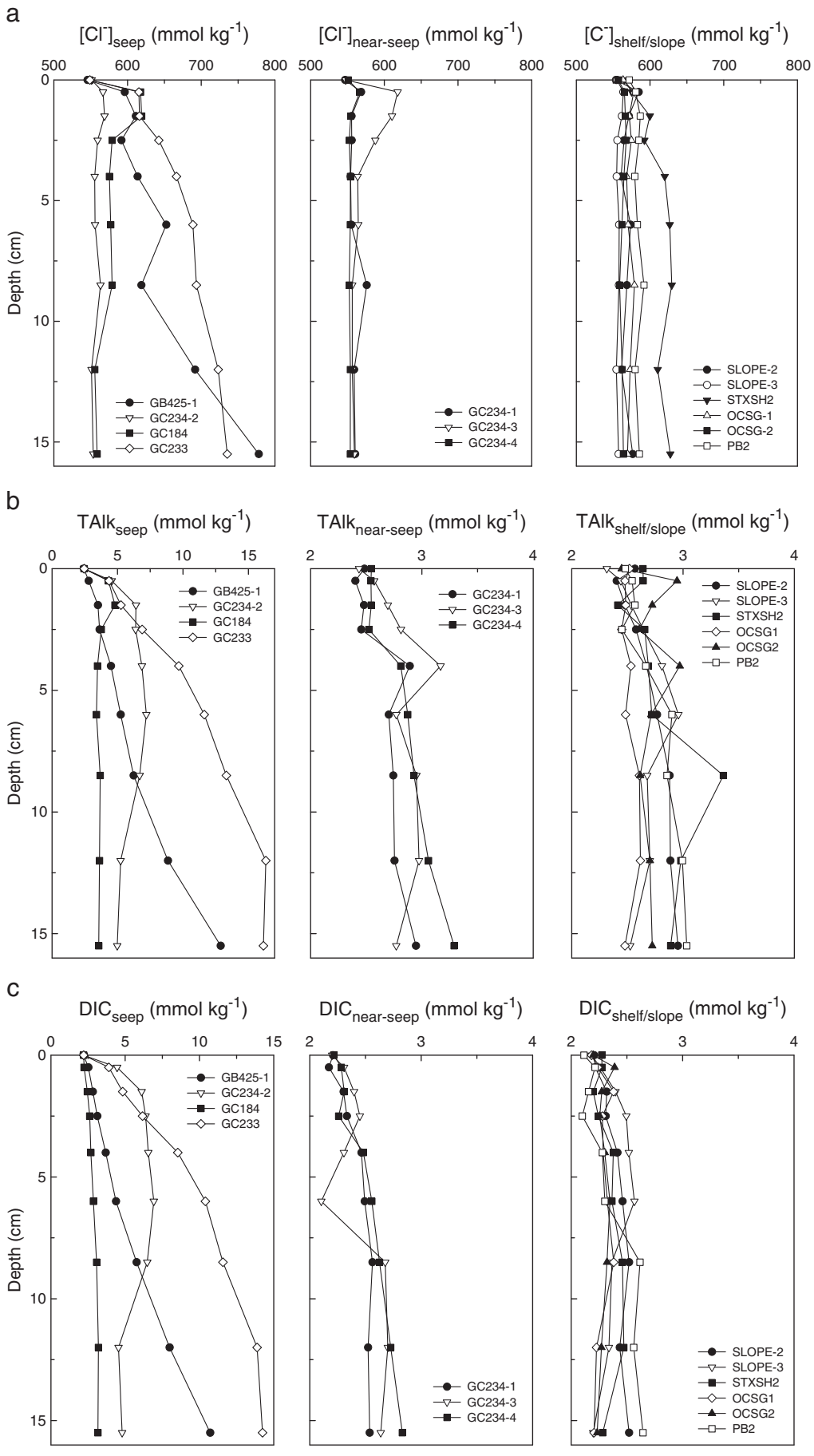

Author's personal copy

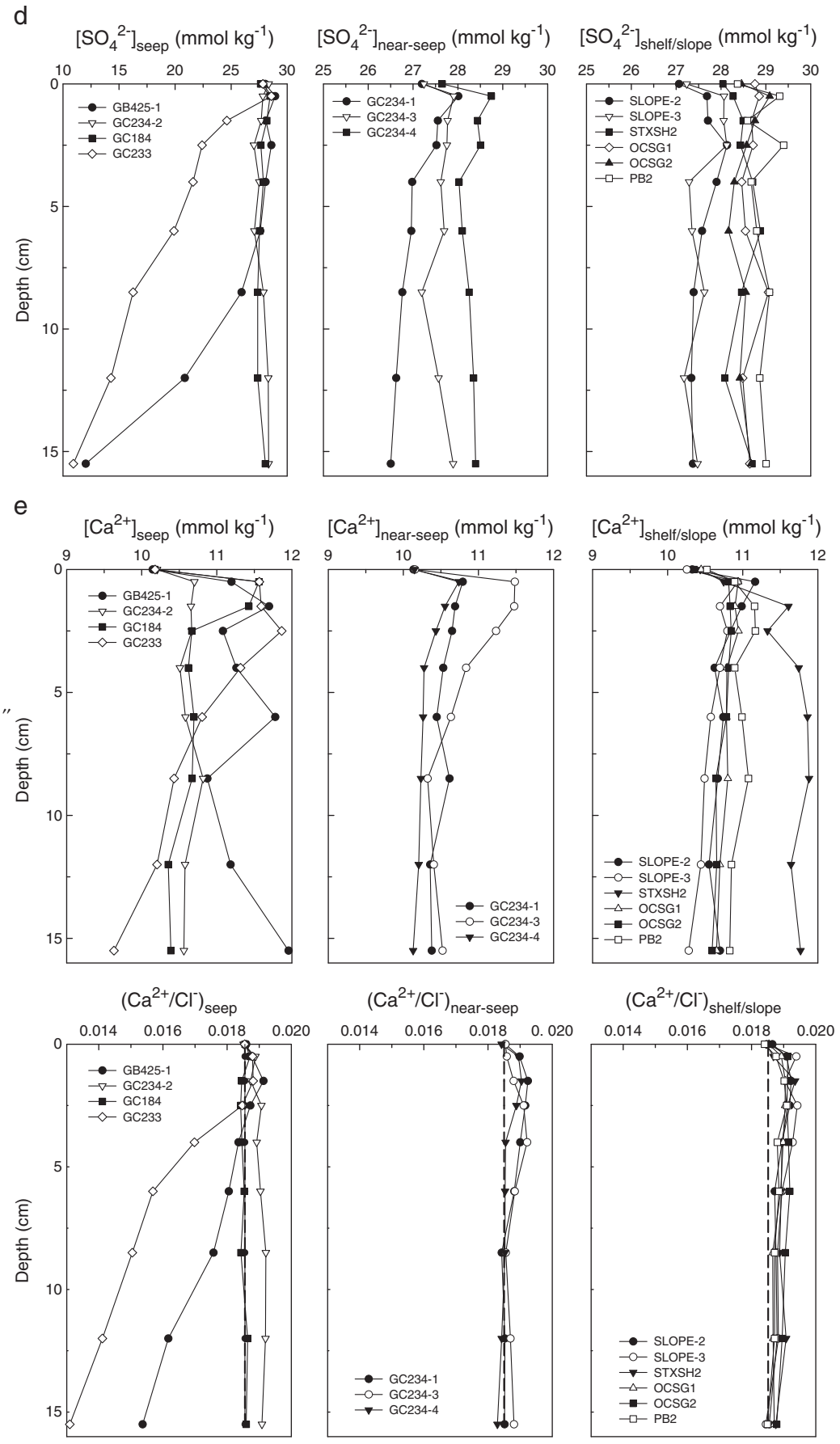

Fig. 4. Profiles of pore-water (a) chloride, (b) total alkalinity (TAlk), (c) DIC, (d) sulfate, and (e) calcium and Ca^{2+}:Cl^{-} molar ratio.

Author's personal copy

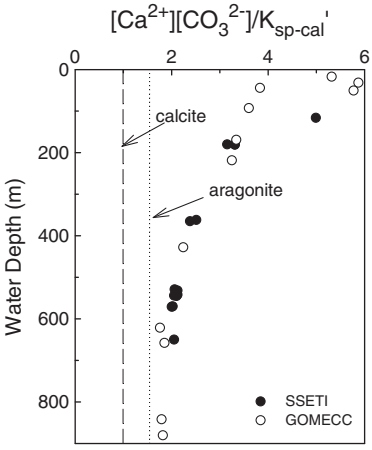

Fig. 5. Bottom water saturation states as represented by the ratio between ionic concentration product ($[Ca^{2+}][CO_3^{2-}]$) and stoichiometric dissolution constant of calcite ($K_{sp\text{-}cal}'$). The filled symbols represent data from this study while the open symbols represent calculated results from our 2007 GOMECC cruise along two north–south transects originated from Galveston, TX and New Orleans, LA (Cai and Hu, unpublished data). The dashed line represents calcite saturation and the dotted line represents aragonite saturation.

values in the water column decreased with depth. At depths greater than 500 m where all the seep and near-seep sediments were located, Ω_{Cal} values in all bottom waters were ~2 (pH value ~7.8). At the shallowest site (116 m), the Parker Bank site (PB2), bottom water Ω_{Cal} value was >4 and pH was the highest as well (8.2). The depth distributions of bottom water pH and Ω_{Cal} are consistent with the water column results that were obtained during the GOMECC (Gulf of Mexico and US East Coast Carbon Program) study at the northern Gulf of Mexico (Fig. 5, Cai and Hu, unpublished data). Note because Ω_{Cal} and Ω_{Arag} values differ by a factor of ~1.5, we chose to describe Ω_{Cal} only in the text, but see Fig. 6b for details.

Unlike the smooth O_2 profiles in the shallow depths (<2 cm), pH profiles were more variable (Fig. 6a) especially in deeper sediments, which reflect significant sediment heterogeneity. Such heterogeneity was also indicated by the occasional mismatches between profiles measured using microelectrode and mini-electrode (punch-in, data not shown). Overall, pH values decreased right below the sediment–water interface, after which pH increased at various extents in the seep and near-seep sediments, but maintained at relatively low values in the shelf-and-slope sediments. One exception was observed in the GC234-2 sediments, where only a pH profile from a mini-electrode was available. At this site, pH showed an initial increase then gradually decreased to ~7.2 at the core bottom. Variations of pH were consistent with calculated pore-water saturation states (Fig. 6b). In both the seep and near-seep sites, initial supersaturation in bottom waters was followed by a sharp decrease in the Ω_{Cal} values immediately below the sediment–water interface, to as low as ~50% of calcite saturation (0.5 Ω_{Cal}). Furthermore, the undersaturation window defined as the length of the undersaturated depth range (e.g., L_{Cal} for calcite and L_{Arag} for aragonite, Table 4) was much narrower in the seep sediments (0–2 cm), compared with that in the near-seep sediments (from 0 to >5 cm) (Fig. 6b). Below the undersaturation window, pore-water saturation states either returned to supersaturation with respect to aragonite (GC184, GC233, and GC234-4) or ended up in an apparent equilibrium with calcite at the core bottoms (GB425-1, GC234-1, GC234-2). In comparison, pore-water Ω_{Cal} values in the shelf-and-slope sediments were less variable. Ω_{Cal} first decreased (usually reached below unity within ~2 cm), then the pore water reached apparent equilibrium with respect to either aragonite (PB2, OCSG2, SLOP-2, SLOPE-3) or calcite (OCSG-1) (Fig. 6b). Note that STXSH2 pore waters had a slight Ω_{Cal} increase following its initial decrease below the sediment–water interface.

4. Discussion

4.1. Sediment porosity

Porosities decreased dramatically along depth in the upper centimeters of the sediment column at the seep sites. Greater porosity decrease may indicate more efficient compaction during sediment burial process (Berner, 1980). On the other hand, possible authigenic carbonate formation that is caused by accumulation of alkalinity produced in anaerobic respirations (Botz et al., 1988; Formolo et al., 2004; Naehr et al., 2007; Ussler and Paull, 2008) may also occupy sediment pore space. Decrease in porosity indicates a reduction in sediment openness, which would subsequently lead to more sluggish exchange between pore water and bottom water by reducing molecular diffusion and advection. As a result, buildup of metabolites from anaerobic respiration (i.e., alkalinity from anaerobic respiration) could occur, leading to elevated carbonate saturation state (Mucci et al., 2000; Formolo et al., 2004) and thus better preservation conditions for carbonate shells; although note bioturbation and bioirrigation could potentially enhance pore-bottom water exchange (see Section 4.3).

4.2. Benthic respiration and carbonate dissolution

Since the bottom waters were all well-oxygenated (Fig. 2) and there was no apparent depletion of sulfate in pore waters (e.g., Fig. 4d), oxygen is expected to be the ultimate electron acceptor in organic matter remineralization (Martin and Sayles, 2004), although note the two profiles of low $[SO_4^{2-}]$ (GB425-1 and GC233) were found to be caused by mixing between bottom seawater and sulfate-depleted brine water (see Hu et al., 2010). Therefore oxygen consumption rate can be used as a first-order approximate for sedimentary respiration rate (e.g., Martin and Sayles, 2004). For the shelf-and-slope (i.e., regular marine) sediments, diffusive O_2 uptake decreased with increasing water depth (Table 3). This is consistent with decreasing metabolic rate as a result of decreasing organic carbon supply from surface production as the sampling sites move further away from the coastline. However, on a broader scale, for all sediment groups in this study, diffusive oxygen uptake decreased in the order of seep, near-seep, and shelf-and-slope sediments corresponding to the order in oxygen penetration depths (Table 3). This trend is expected given the potentially greater organic carbon supply in the seep-related environments, where organic carbon associated with seep activities not only export fossil carbon to the surface sediment and water column (e.g., Table 2), but also export reduced reactants (e.g., reduced sulfur) that are used to support the growth of lush chemosynthetic communities (Sassen et al., 1999; Arvidson et al., 2004).

If we assume that calcium flux at the sediment–water interface represents the depth-integrated net carbonate dissolution rate (i.e., $CaCO_3$ is the dissolving mineral, Jahnke and Jahnke, 2000), then our sampling sites at the northern Gulf of Mexico have higher carbonate dissolution rates (3.1–10.9 mmol $m^{-2} d^{-1}$, Table 3) than those in most other ocean margin sediments that have been studied. For example, Mucci et al. (2000) observed carbonate dissolution flux of 0.1–2.6 mmol $m^{-2} d^{-1}$ in the eastern Canada continental shelf; Jahnke and Jahnke (2000) reported a carbonate dissolution flux of 0.3–3.0 mmol $m^{-2} d^{-1}$ in the Middle Atlantic Bight slope sediments. On the other hand, our calculated carbonate dissolution rates are consistent with those from our previous study (1.1–5.8 mmol $m^{-2} d^{-1}$) that examined both seep and near-seep sediments (Cai et al., 2006). If plotting carbonate dissolution flux vs. diffusive oxygen flux (Fig. 7), it appears that carbonate dissolution roughly follows the diffusive oxygen consumption, although the linear regression between these two quantities is not statistically significant ($r = 0.36$, $P = 0.22$). A caveat, however, should be pointed out in using

Author's personal copy

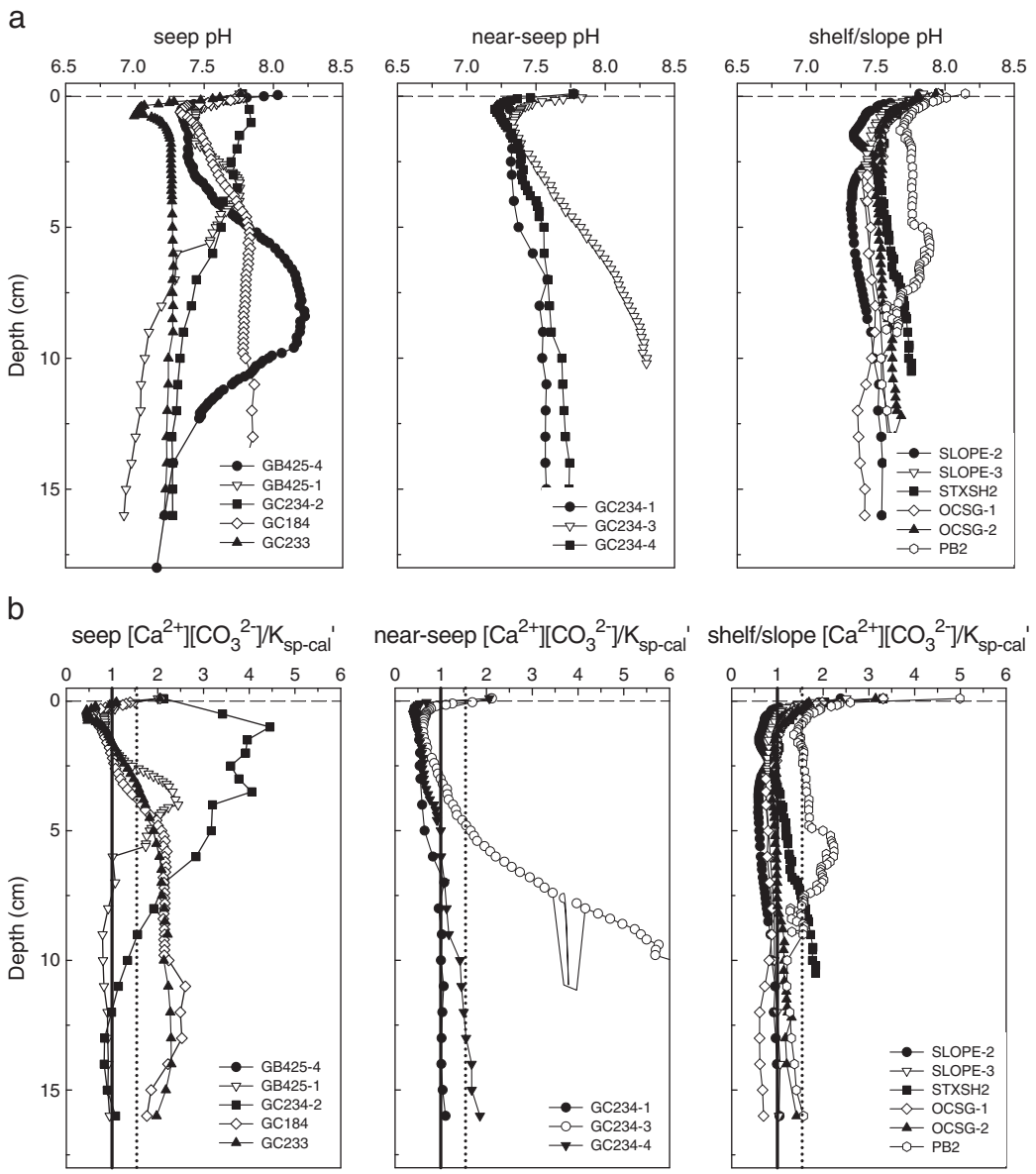

Fig. 6. (a) Pore-water pH profiles, (b) pore-water carbonate saturation state with respect to calcite. See text for details about the method used for calculating carbonate saturation states. Note in the upper sediment column the higher resolution profiles were taken using the microelectrodes and the lower resolution profiles in deeper sediments were taken using a mini-electrode (punch-in), subsequently carbonate saturation state profiles in (b) also reflect the electrode change. The vertical lines represent saturation levels of calcite (solid) and aragonite (dotted).

diffusive fluxes to represent benthic fluxes. An earlier study (Hu et al., 2010) indicates that pore-water advection (either downward or upward) dominates pore-water movements at two of the active seep-influenced sites (GB425-1 and GC233), thus the diffusive fluxes calculated here could only represent the lower limits of the total dissolution fluxes in the seep sites. This likely contributes to the fact that the correlation coefficient between the dissolution rates and O_2 diffusive fluxes is not high (Fig. 7).

4.3. An indicator for carbonate preservation potential—carbonate dissolution index

Although bottom water saturation state decreased with water depth (Fig. 5), the value remained above aragonite saturation in the northern Gulf of Mexico continental shelf and slope area within the water depth up to 1000 m. Therefore bottom water alone is not expected to affect carbonate preservation/dissolution. However, in spite of the supersaturated bottom waters, all SSETI sediment pore waters exhibited various extents of undersaturation with respect to both aragonite and calcite at different depth intervals (Fig. 6b). This undersaturation can be attributed to acid production from sedimentary respiration processes. Direct reactions involved in generating acid include aerobic organic carbon respiration product (i.e., CO_2) and to a much less extent, a small degree of sulfate reduction (~3% of seawater sulfate reduction, Morse and Mackenzie, 1990; Stoessell, 1992; Boudreau and Canfield, 1993). At the same time, aerobic oxidation of reduced species (e.g., sulfide, reduced metals such as Fe^{2+} and Mn^{2+}) that move upward through either diffusion or bioturbation from sediment depth also generates protons, which suppress both pore-water pH and saturation state within the oxygenated depths (Canfield et al., 1993; Cai et al., 2006; Soetaert et al., 2007).

Oxidation of reduced species by oxygen can only occur within the oxygen penetration zone (Fig. 3). The pore-water saturation state below this zone will be controlled by anaerobic reactions and the extent of pore-water bioirrigation mediated by benthic organisms. With the progression of anaerobic organic carbon oxidation, buildup of pore-water TAlk eventually could lead to supersaturation and authigenic

Author's personal copy

carbonate production (Boudreau and Canfield, 1993; Mucci et al., 2000). Therefore, despite limited range of oxygen penetration (within 2 cm), oxygen penetration depth and the length of the pore-water undersaturation window (e.g., L_{Cal} in Table 4) in these three sediment groups correlate well ($r=0.72$, $P=0.008$, Fig. 8), i.e., a wider pore-water undersaturation window can be correlated to deeper oxygen penetration. This correlation indicates increasing rates of organic carbon respiration and reoxidation of reduced species in the order of shelf-and-slope, near-seep, and seep sites. High diagenetic reaction rates not only promote high oxygen consumption rate and thus reduce oxygen penetration depth, but also raise pore-water pH and saturation states in deeper sediments where anaerobic reactions are dominant. Note in PB2 an apparent increase in saturation state at the 5–7 cm interval indicates possible bioirrigation that transports supersaturated bottom water into the sediment (Fig. 6a & b).

Another useful indicator for carbonate dissolution is pore-water $[Ca^{2+}]$ change relative to bottom-water value (e.g., Aller, 1982; Walter and Burton, 1990; Green and Aller, 1998, 2001). In our case, however, pore-water $[Cl^-]$ also varied, thus we chose to use $[Ca^{2+}]$:$[Cl^-]$ ratios to illustrate net carbonate dissolution (lower panel in Fig. 4e). Along the continental margin of the northern Gulf of Mexico, the three sediment groups clearly demonstrated distinctly different carbonate dissolution behaviors. Carbonate dissolution apparently occurred throughout the sampled depth range in the shelf-and-slope sediments, which all had elevated $[Ca^{2+}]$:$[Cl^-]$ ratios compared to bottom waters. In the near-seep sediments, dissolution can be seen in the upper ~5–10 cm. In contrast, a very restricted carbonate dissolution zone (upper ~2 cm) existed in the seep sediments (except in GC234-2 where elevated $[Ca^{2+}]$:$[Cl^-]$ ratio was observed). Note here that significant decreases in the $[Ca^{2+}]$:$[Cl^-]$ ratio along depth with increasing $[Cl^-]$ in GB425-1 and GC233 suggest a brine-seawater mixing scenario, because the underlying brines have lower $[Ca^{2+}]$:$[Cl^-]$ ratios than normal seawater (Joye et al., 2005). These different levels of pore-water $[Ca^{2+}]$ increase are consistent with calculated pore-water saturation states (Fig. 6b).

Pore-water undersaturation is important in terms of understanding carbonate shell preservation because dissolution is one of the most important reasons for carbonate shell breakage and carbonate loss, due to the fact that dissolving the hard part of the carbonate shell weakens the shell strength thus makes them susceptible to further physical abrasion and breakage (e.g., Walker and Goldstein, 1999; Sanders, 2003; Cai et al., 2006). In light of the carbonate dissolution conditions observed in these sediments, carbonate loss from shells may be qualitatively estimated. In the top 17 cm of the shelf-and-slope sediments, continuous carbonate dissolution is expected to occur, especially for carbonate shells made of aragonite. Due to a shortened or compressed undersaturation window in the near-seep sediments compared to the shelf-and-slope sediments, carbonate dissolution should occur only in the upper 5–10 cm. In the seep sediments, drastic carbonate undersaturation immediately below the sediment–water interface is the most important driving force for carbonate dissolution. However, below this undersaturation zone (Fig. 6b), rapid buildup of carbonate alkalinity along with elevated pore-water carbonate saturation states could inhibit further carbonate dissolution and may lead to shell preservation and even authigenic carbonate formation.

If carbonate undersaturation determines the rate of carbonate loss through dissolution, the time needed for a shell that falls onto the surface sediments to pass through the undersaturation window depends on the sedimentation rate (Cai et al., 2006). Once the shell escapes from this undersaturation window, the remaining part will be preserved eventually. Therefore shell preservation ultimately relies on the interplay between pore-water saturation and sedimentation rate (Emerson and Archer, 1990).

If we assume that the pore water maintains at a steady-state, then the total loss of carbonate (here defined as carbonate dissolution index, or CDI) through dissolution can be expressed as:

$$CDI \int_0^t R_t dt \tag{2}$$

in which t is the time it takes for a shell to pass through the undersaturation window (L, which is determined from the pore water saturation profile in Fig. 6b), and R_t is dissolution rate. t and R_t can be expressed as functions of sedimentation rate (ω) and pore-water saturation state (Ω) (Keir, 1980), respectively:

$$t = \frac{L}{\omega} \tag{3}$$

and

$$R_t = k(1-\Omega_t)^n \tag{4}$$

where k is the dissolution rate constant, and n is the reaction order (Walter and Morse, 1985).

Table 4
Sedimentation rates (ω)[a], length of undersaturation window with respect to calcite (L_{Cal}) and aragonite (L_{Arag}), and carbonate dissolution index with respect to calcite (CDI_{Cal}) and aragonite (CDI_{Arag}).

Sediment type	Site ID	Ω (cm yr^{-1})	L_{Cal} (cm)	CDI_{Cal}	L_{Arag} (cm)	CDI_{Arag}
Seep	GB425-4	0.043 ± 0.004	nd[b]	nd	nd	nd
	GB425-1	0.014 ± 0.001	1.45	195	2.45	11,042
	GC234-2	0.058 ± 0.005	3.00	132	7.05[c]	7339
	GC184	0.074 ± 0.004	1.95	368	3.75	3767
	GC233	0.030 ± 0.006	1.45	1772	3.15	9018
	Average	0.044 ± 0.023	1.96 ± 0.73	617 ± 777	4.09 ± 2.01	7792 ± 3081
Near-seep	GC234-4	0.062 ± 0.002	4.95	3529	12.95	17842
	GC234-3	0.028 ± 0.002	2.80	1770	4.70	15,931
	GC234-1	0.050 ± 0.002	5.50	5849	15.50[c]	32,349
	Average	0.047 ± 0.017	4.42 ± 1.43	3716 ± 2046	11.05 ± 5.65	21,861 ± 9165
Shelf-and-slope	SLOPE-3	0.190 ± 0.010	11.40	143	14.50[c]	6264
	STXSH2	0.247 ± 0.018	2.05	1	7.35	878
	OCSG-2	0.081 ± 0.005	6.30	15	15.70[c]	7351
	OCSG-1	0.086 ± 0.005	14.50[c]	2459	15.75[c]	22,889
	SLOPE-2	0.188 ± 0.007	13.70	1182	15.80[c]	10,103
	PB2	0.189 ± 0.018	ss[d]	ss[d]	8.10[c]	247
	Average	0.163 ± 0.066	9.59 ± 5.29	760 ± 1070	12.87 ± 4.02	7955 ± 8251

[a] Due to changing sediment porosities with depth, mass-depth sedimentation rates were first calculated using the method in Chanton et al. (1983) assuming a dry sediment density 2.5 g cm^{-3}. Then this rate was converted to length-based sedimentation rate using the predicted porosity at infinite depth (Eq. (1)) assuming a steady-state compaction.
[b] nd denotes no data.
[c] Lower boundary of the undersaturation window is the bottom of the core (16 cm).
[d] ss denotes pore-water supersaturation.

Author's personal copy

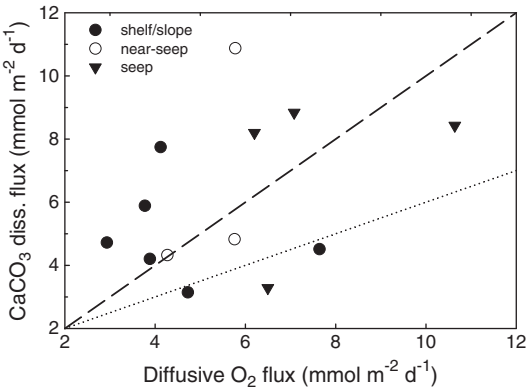

Fig. 7. Diffusive carbonate dissolution flux vs. diffusive oxygen uptake rate. The dashed line represents a 1:1 stoichiometry for the simplified reaction with CH_2O as the organic carbon source (carbon valent = 0) $CaCO_3 + O_2 + CH_2O \rightarrow Ca^{2+} + 2HCO_3^-$, whereas the dotted line represents a 1:2 stoichiometry for the reaction with methane as the organic carbon source (carbon valent = −4) $CaCO_3 + 2O_2 + CH_4 \rightarrow Ca^{2+} + 2HCO_3^-$.

A number of studies have examined carbonate dissolution kinetics using both synthetic and natural carbonate materials (Berner and Morse, 1974; Keir, 1980; Walter and Morse, 1985; Berelson et al., 1994; Hales and Emerson, 1997; Morse and Arvidson, 2002; Gehlen et al., 2005). Controlling factors including carbonate particle size (or reactive surface area, see Walter and Morse, 1984; Morse and Arvidson, 2002), presence of foreign ions (Morse and Arvidson, 2002) and organic matter (Morse, 1974), all affect carbonate dissolution kinetics even though detailed mechanisms are not entirely clear (Morse and Arvidson, 2002). Here we chose to use the values reported in Walter and Morse (1985) based on their dissolution studies using shallow marine biogenic carbonate minerals. The values of n and $\log(k)$ for calcite and aragonite are 2.86 and 2.82 μmol g^{-1} h^{-1}, and 2.48 and 2.89 μmol g^{-1} h^{-1}, respectively. Assuming that the carbonate materials under examination at these sites had the same set of k and n values for calcite and aragonite, then based on sedimentation rates using ^{210}Pb chronology (Luo, unpublished data, Table 4), we then estimated the semi-quantitative parameter—CDI that may be used to describe the extent of carbonate dissolution in these sediments, and the results are shown in Table 4. In calculating the CDI values, we converted the dissolution rate constants k using $CaCO_3$ molecular weight of 100 g mol^{-1}, thus the CDI values are unitless.

Calculated CDI values for both calcite and aragonite are significantly different among the three sediment groups (i.e., seep, near-seep, and shelf-and-slope, Table 5). Multiple pairwise t-tests suggest

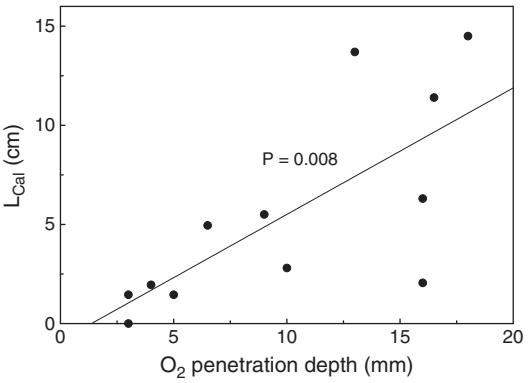

Fig. 8. The width of calcite undersaturation window (L_{Cal}, from Table 4) vs. oxygen penetration depth. Note GC234-2 pore water saturation is initially supersaturated below sediment–water interface and then decreases to undersaturation at below 9 cm depth (Fig. 6b). The deep undersaturation presumably is not caused by diffusive O_2 input at surface sediment (oxygen penetration depth is 3 mm), thus we use $L_{Cal} = 0$ for this site.

Table 5
The results of two-tailed t-test on the CDI_{Cal} and CDI_{Arag} values (as shown in Table 4) from the three groups of sediments.

		t	df	P
CDI_{Cal}	Seep vs. near-seep	2.84	5	0.04
	Shelf-and-slope vs. near-seep	2.75	6	0.03
	Seep vs. shelf-and-slope	0.22	7	0.83
CDI_{Arag}	Seep vs. near-seep	2.94	5	0.03
	Shelf-and-slope vs. near-seep	2.31	7	0.05[a]
	Seep vs. shelf-and-slope	0.04	8	0.97

[a] The t value here (2.31) for the comparison between the shelf-and-slope vs. near-seep sediments is slightly smaller than the critical t value (2.36) at the degree of freedom of 7.

that the shelf-and-slope sediments and the seep sediments both have lower CDI values than those of the near-seep sediments. There was no significant difference between the shelf-and-slope and the seep sediments (Table 5). Note that the t-test between the two sets of CDI_{Arag} values obtained from the shelf-and-slope sediments and the near-seep sediment suggests a weak difference (Table 5 footnote) if $\alpha = 0.05$ was chosen. Nevertheless, it appears that both the shelf-and-slope and the seep sediments have similar capabilities in dissolving carbonate minerals (for both calcite and aragonite) while the near-seep sediments are the most corrosive. The similarity in CDI values of these two groups of sediments (i.e., shelf-and-slope and seep) can be explained by a combined effect of pore-water saturation state (Ω) and the time needed for a shell to pass through the undersaturation window, i.e., the seep sites had much lower pore-water saturation states although the undersaturation windows were narrower when compared to the shelf-and-slope sites. Thus while these two groups have similar CDI over an integrated depth of the top 17 cm, the mode of dissolution and their time course are very different. Hence, we would expect shells to experience faster dissolution within a short time scale at the seep sites (due to low saturation state and high instantaneous dissolution rate within the undersaturation window) while shells at the shelf-and-slope sites to experience slower and longer-term dissolution, and the time scale will depend on the sedimentation rate. Therefore, we also conjecture that smaller shells (or shells that have more soluble aragonite) may not be able to "survive" fast dissolution at the seeps sites, whereas larger shells (or shells composed of calcite) would.

Moreover, because most of the seep sediments have narrow undersaturation windows (Table 4), beyond which pore water tends to be supersaturated with respect to both calcite and aragonite (pore-water saturation state in the deeper depth at GC234-2 depth is difficult to predict since tubeworms were present nearby), it is then reasonable to expect that a carbonate shell should be preserved once it passes through this narrow undersaturation window (Cai et al., 2006). Furthermore, despite the fact that the shelf-and-slope and the seep sediments may have similar carbonate-dissolving capability in the sampled depth interval, deeper pore-water undersaturation beyond our measured depth range at the shelf-and-slope sites potentially could lead to additional dissolution (especially for aragonite) during the burial process, given that all shelf-and-slope sites except STXSH2 had undersaturated pore waters with respect to aragonite.

According to our calculation, average CDI values in the near-seep sites are about five (for calcite) and two (for aragonite) times higher than those from both the shelf-and-slope and the seep sites. The reason for enhanced dissolution at the near-seep sites can be explained by a relatively wider undersaturation window (2–3 times) but similar extent of undersaturation and sedimentation rates as those of the seep sites. The shortened undersaturation window at the seep sites may be explained by more abundant input of organic matter from deep sediments (Table 2), which causes a more compressed redox reaction zone.

Based on the above discussion, we conjecture that carbonate shells may be better preserved in environments with high organic matter

Author's personal copy

input rates, the latter are usually associated with high sedimentation rates (e.g., Burdige, 2006). Although with similar apparent sedimentation rates at both the near-seep and the seep sites, clearly the seep sites are more enriched in organic carbon (Table 2). On the other hand, the presence of oxygen in bottom water should also play an important role in determining carbonate dissolution and preservation, because the existence of the undersaturation window is caused by both aerobic respiration and reoxidation of reduced species that are brought up from subsurface sediments (with or without bioturbation and advection). For example, Ku et al. (1999) demonstrated that redox cycling between sulfate and sulfide causes syndepositional dissolution of carbonate in an open carbonate sedimentary system in the Florida Keys.

Taken together, we conclude that the seep sediments may have the highest preservation potential for carbonate shells due to their low CDI values (thus less overall dissolution) if the shells can survive the initial fast dissolution due to a sharply decreased saturation. A number of factors control the likelihood of shell preservation, including mineralogy and shell microstructure (Cai et al., 2006). Cai et al. (2006) showed that the seep sites were more corrosive to carbonate shells. However, the difference between this study and Cai et al. (2006) is that this study examines the taphonomic effect below the sediment–water interface (i.e., after a shell survives the initial dissolution immediately below the sediment–water interface and then enters our studied upper sediment column). In contrast, what was observed in Cai et al. (2006) revealed taphonomic changes that occurred at or near the sediment–water interface upon retrieval, where corrosive pore water was present immediately underneath in the seep sediments. In fact, the concept of CDI is consistent with the hypothesis in Cai et al. (2006) that long term burial with taphonomic change may be different from the observed pre-burial changes obtained in our SSETI experiment, given the distinctively different geochemical properties throughout the upper centimeters of sediment column. Upon deep burial in the seep sediments, excess alkalinity produced by remineralization of sedimentary organic carbon as well as fossil carbon could also lead to formation of authigenic carbonate (Botz et al., 1988; Formolo et al., 2004; Gieskes et al., 2005; Naehr et al., 2007). This then facilitates eventual preservation of carbonate shells buried in this type of environment.

Here we note that our calculated CDI values are likely conservative estimates because we did not consider possible bioturbation caused by benthic infauna in our calculations. The presence of bioturbation could repeatedly expose buried shells to undersaturated pore waters for extended periods of time (e.g., Aller, 1982; Sanders, 2003). On the other hand, however, because both the rate constants (k) and reaction order (n) are based on measured dissolution kinetics of carbonate materials that have a particle size ranging between 37 and 125 μm (Walter and Morse, 1985), these CDI values can only be considered as relative quantities since naturally occurring carbonate shells have both larger sizes and intrinsic organic matrices (e.g., Sanders, 2001), which potentially would lead to much slower dissolution kinetics. Nevertheless, the underlying chemistry (i.e., the reaction rate law) that is integrated over time (based on sedimentation) will provide us a useful proxy in exploring the potential of carbonate material dissolution in marine sediments in a general sense.

Finally, since all pore-water pH measurements were limited to the upper 17 cm of sediments in this study, subsequent pore-water saturation and CDI calculations are thus limited in this depth range. Therefore the CDI values are only indicative for the extent of carbonate dissolution in the depth range under examination. Given different sedimentation rates observed in these sediments, we should bear in mind that the same depth range across these different sedimentary settings represents different time scales depending on the sedimentation rate (Table 4). Moreover, since the SSETI project deployed carbonate shells in these different environments less than two decades ago and many shells were still at the sediment–water interface upon retrieval, clear correlation between CDI and carbonate taphonomic changes from these deployed samples may not be evident (Hu et al., in preparation) because our CDI here represent an integrated taphonomic change over the studied sediment column. Instead, buried shells in deeper depths should be used to validate this hypothesis.

5. Summary

Through examining the geochemistry of the sediments from the northern Gulf of Mexico, we identified three groups of sediments (i.e., seep, near-seep, and continental shelf-and-slope) based on their locations and geochemical characteristics (oxygen uptake/penetration depth, pore-water saturation states, and carbonate dissolution fluxes). Diffusive oxygen uptake rate increased in the order of shelf-and-slope, near-seep, and seep sediments with increasing contribution of fossil carbon; however, carbonate dissolution fluxes did not show clear correlation with oxygen uptake rate, presumably caused by non-diffusive solute exchange (e.g., bioturbation, bioirrigation, and advection) between the bottom water and the pore water.

Using calculated pore-water saturation indices with respect to two common marine carbonate minerals (i.e., aragonite and calcite) and sedimentation rates, we defined a parameter—carbonate dissolution index (CDI) to predict the carbonate preservation potential during the taphonomic process. Our limited dataset suggests that both the seep and the shelf-and-slope sediments may have higher carbonate preservation potential than the near-seep sediments. This conclusion is broadly consistent with the hypothesis in Cai et al. (2006) that burial process may be different from the observed pre-burial changes, which actually revealed more shell destruction in the surface of seep sediments. Therefore, further quantitative studies need to be carried out to verify the relationship between the CDI and the extent of taphonomic changes of carbonate shells buried at sediment depth.

Acknowledgments

Funding for this study was provided by the National Science Foundation and the National Undersea Research Program to the Shelf-Slope Experimental Taphonomy Initiative (SSETI). We thank the ship board scientific party and the captain and crew of the *R/V Seaward Johnson* and the deep submerge vehicle *Johnson Sea-Link* for their help with sample collections. Special thanks are also extended to G. Han for her help with pore-water analyses; T. Maddox for helping with analyzing sedimentary organic carbon and carbonate concentrations; Z. Huang and F. Wang for their assistance with sediment core processing; and E. Powell for constructive comments on an earlier draft of this manuscript. The guest editor for this special issue—S. Walker and two anonymous reviewers offered insightful comments on an earlier version of this paper which helped to improve the quality of this work.

References

Alexandersson, E.T., 1975. Etch patterns on calcareous sediment grains: petrographic evidence of marine dissolution of carbonate minerals. Science 189, 47–48.
Alexandersson, E.T., 1978. Destructive diagenesis of carbonate sediments in the eastern Skagerrak, North Sea. Geology 6, 324–327.
Aller, R.C., 1982. Carbonate dissolution in nearshore terrigenous muds: the role of physical and biological reworking. Journal of Geology 90, 79–95.
Arvidson, R.S., Morse, J.W., Joye, S.B., 2004. The sulfur biogeochemistry of chemosynthetic cold seep communities, Gulf of Mexico, USA. Marine Chemistry 87, 97–119.
Berelson, W.M., Hammond, D.E., McManus, J., Kilgore, T.E., 1994. Dissolution kinetics of calcium carbonate in equatorial Pacific sediments. Global Biogeochemical Cycles 8, 219–235.
Berner, R.A., 1980. Early diagenesis — a theoretical approach. Princeton Series in Geochemistry. Princeton University Press, Princeton, N.J. 256 pp.
Berner, R.A., Morse, J.W., 1974. Dissolution kinetics of calcium carbonate in seawater IV. Theory of calcite dissolution. American Journal of Science 274, 108–134.
Best, M.M.R., Ku, T.C.W., Kidwell, S.M., Walter, L.M., 2007. Carbonate preservation in shallow marine environments: unexpected role of tropical siliciclastics. Journal of Geology 115, 437–456.
Botz, R., Faber, E., Whiticar, M.J., Brooks, J.M., 1988. Authigenic carbonates in sediments from the Gulf of Mexico. Earth and Planetary Science Letters 88, 263–272.

Author's personal copy

Boudreau, B.P., 1997. Diagenetic Models and Their Implementation — Modelling Transport and Reactions in Aquatic Sediments. Springer. 414 pp.
Boudreau, B.P., Canfield, D.E., 1993. A comparison of closed- and open-system models for porewater pH and calcite-saturation state. Geochimica et Cosmochimica Acta 57, 317–334.
Burdige, D.J., 2006. Geochemistry of Marine Sediments. Princeton University Press. 609 pp.
Cai, W.-J., Reimers, C.E., 1993. The development of pH and pCO_2 microelectrodes for studying the carbonate chemistry of pore waters near the sediment–water interface. Limnology and Oceanography 38, 1762–1773.
Cai, W.-J., Sayles, F.L., 1996. Oxygen penetration depths and fluxes in marine sediments. Marine Chemistry 52, 123–131.
Cai, W.-J., Wang, Y., 1998. The chemistry, fluxes, and sources of carbon dioxide in the estuarine waters of the Satilla and Altamaha Rivers, Georgia. Limnology and Oceanography 43, 657–668.
Cai, W.-J., Chen, F., Powell, E.N., Walker, S.E., Parsons-Hubbard, K.M., Staff, G.M., Wang, Y., Ashton-Alcox, K.A., Callender, W.R., Brett, C.E., 2006. Preferential dissolution of carbonate shells driven by petroleum seep activity in the Gulf of Mexico. Earth and Planetary Science Letters 248, 227–243.
Canfield, D.E., Thamdrup, B., Hansen, J.W., 1993. The anaerobic degradation of organic matter in Danish coastal sediments: iron reduction, manganese reduction, and sulfate reduction. Geochimica et Cosmochimica Acta 57, 3867–3883.
Chanton, J.P., Martens, C.S., Kipphut, G.W., 1983. Lead-210 sediment geochronology in a changing coastal environment. Geochimica et Cosmochimica Acta 47, 1791–1804.
Dickson, A.G., Millero, F.J., 1987. A comparison of the equilibrium constants for the dissociation of carbonic acid in seawater media. Deep Sea Research, Part I: Oceanographic Research Papers 34, 1733–1743.
Emerson, S.R., Archer, D., 1990. Calcium carbonate preservation in the ocean. Philosophical Transactions of the Royal Society of London. Series A: Mathematical and Physical Sciences 331, 29–40.
Formolo, M.J., Lyons, T.W., Zhang, C., Kelley, C., Sassen, R., Horita, J., Cole, D.R., 2004. Quantifying carbon sources in the formation of authigenic carbonates at gas hydrate sites in the Gulf of Mexico. Chemical Geology 205, 253–264.
Gallaway, B.J., Martin, L.R., Howard, R.L., 1988. Northern Gulf of Mexico continental slope study. Annual Report. MMS/GM-87/0060, Minerals Management Service. Gulf of Mexico OCS Regional Office, Metairie, LA.
Gehlen, M., Bassinot, F.C., Chou, L., McCorkle, D., 2005. Reassessing the dissolution of marine carbonates: II. Reaction kinetics. Deep Sea Research, Part I: Oceanographic Research Papers 52, 1461–1476.
Gieskes, J.M., Mahn, C., 2007. Halide systematics in interstitial waters of ocean drilling sediment cores. Applied Geochemistry 22, 515–533.
Gieskes, J., Mahn, C., Day, S., Martin, J.B., Greinert, J., Rathburn, T., McAdoo, B., 2005. A study of the chemistry of pore fluids and authigenic carbonates in methane seep environments: Kodiak Trench, Hydrate Ridge, Monterey Bay, and Eel River Basin. Chemical Geology 220, 329–345.
Grasshoff, K., Kremling, K., Ehrhardt, M., 1999. Methods of Seawater Analysis. Wiley-VCH. 600 pp.
Green, M.A., Aller, R.C., 1998. Seasonal patterns of carbonate diagenesis in nearshore terrigenous muds: relation to spring phytoplankton bloom and temperature. Journal of Marine Research 56, 1097–1123.
Green, M.A., Aller, R.C., 2001. Early diagenesis of calcium carbonate in Long Island Sound sediments: benthic fluxes of Ca^{2+} and minor elements during seasonal periods of net dissolution. Journal of Marine Research 59, 769–794.
Green, M.A., Aller, R.C., Aller, J.Y., 1992. Experimental evaluation of the influences of biogenic reworking on carbonate preservation in nearshore sediments. Marine Geology 107, 175–181.
Green, M.A., Aller, R.C., Aller, J.Y., 1993. Carbonate dissolution and temporal abundances of Foraminifera in Long Island Sound sediments. Limnology and Oceanography 38, 331–345.
Hales, B., Emerson, S., 1997. Evidence in support of first-order kinetics of calcite in seawater. Earth and Planetary Science Letters 148, 317–327.
Hu, X., Cai, W.-J., Wang, Y., Luo, S., Guo, X., 2010. Pore-water geochemistry of two contrasting brine-charged seep sites in the northern Gulf of Mexico continental slope. Marine Chemistry 118, 99–107.
Hu, X., Cai, W.-J., Powell, E.N., Ashton-Alcox, K.A., Parsons-Hubbard, K.M., in preparation. Geochemical controls on carbonate shell taphonomy in the northern Gulf of Mexico sediments.
Jahnke, R.A., Jahnke, D.B., 2000. Rates of C, N, P and Si recycling and denitrification at the US Mid-Atlantic continental slope depocenter. Deep Sea Research, Part I: Oceanographic Research Papers 47, 1405–1428.
Joye, S.B., Boetius, A., Orcutt, B.N., Montoya, J.P., Schulz, H.N., Erickson, M.J., Lugo, S.K., 2004. The anaerobic oxidation of methane and sulfate reduction in sediments from Gulf of Mexico cold seeps. Chemical Geology 205, 219–238.
Joye, S.B., MacDonald, I.R., Montoya, J.P., Peccini, M., 2005. Geophysical and geochemical signatures of Gulf of Mexico seafloor brines. Biogeosciences 2, 295–309.
Keir, R.S., 1980. The dissolution kinetics of biogenic calcium carbonates in seawater. Geochimica et Cosmochimica Acta 44, 241–252.
Kidwell, S.M., Best, M.M.R., Kaufman, D.S., 2005. Taphonomic trade-offs in tropical marine death assemblages: differential time averaging, shell loss, and probable bias in siliciclastic vs. carbonate facies. Geology 33, 729–732.
Ku, T.C.W., Walter, L.M., Coleman, M.L., Blake, R.E., Martini, A.M., 1999. Coupling between sulfur recycling and syndepositional carbonate dissolution: evidence from oxygen and sulfur isotope composition of pore water sulfate, South Florida Platform, U.S.A. Geochimica et Cosmochimica Acta 63, 2529–2546.
Lewis, E., Wallace, D., 1998. Program developed for CO_2 system calculations. ORNL/CDIAC-105. Carbon Dioxide Information Analysis Center, Oak Ridge National Laboratory, U.S. Department of Energy, Oak Ridge, Tennessee.
Martin, W.R., Sayles, F.L., 2004. Organic matter cycling in sediments of the continental margin in the northwest Atlantic Ocean. Deep Sea Research, Part I: Oceanographic Research Papers 51, 457–489.
Mehrbach, C., Culberson, C.H., Hawley, J.E., Pytkowicz, R.M., 1973. Measurement of the apparent dissociation constants of carbonic acid in seawater at atmospheric pressure. Limnology and Oceanography 18, 897–907.
Morse, J.W., 1974. Dissolution kinetics of calcium carbonate in seawater V. Effects of natural inhibitors and the position of the lysocline. American Journal of Science 274, 638–647.
Morse, J.W., Arvidson, R.S., 2002. The dissolution kinetics of major sedimentary carbonate minerals. Earth-Science Reviews 58, 51–84.
Morse, J.W., Beazley, M.J., 2008. Organic matter in deepwater sediments of the Northern Gulf of Mexico and its relationship to the distribution of benthic organisms. Deep Sea Research, Part II: Topical Studies in Oceanography 55, 2563–2571.
Morse, J.W., Mackenzie, F.T., 1990. Geochemistry of sedimentary carbonates. Developments in Sedimentology, 48. Elsevier. 707 pp.
Mucci, A., 1983. The solubility of calcite and aragonite in seawater at various salinities. American Journal of Science 283, 780–799.
Mucci, A., Sundby, B., Gehlen, M., Arakaki, T., Zhong, S., Silverberg, N., 2000. The fate of carbon in continental shelf sediments of eastern Canada: a case study. Deep Sea Research, Part II: Topical Studies in Oceanography 47, 733–760.
Muramatsu, Y., Doi, T., Tomaru, H., Fehn, U., Takeuchi, R., Matsumoto, R., 2007. Halogen concentrations in pore waters and sediments of the Nankai Trough, Japan: implications for the origin of gas hydrates. Applied Geochemistry 22, 534–556.
Naehr, T.H., Eichhubl, P., Orphan, V.J., Hovland, M., Paull, C.K., Ussler, Iii.W., Lorenson, T.D., Greene, H.G., 2007. Authigenic carbonate formation at hydrocarbon seeps in continental margin sediments: a comparative study. Deep Sea Research, Part II: Topical Studies in Oceanography 54, 1268–1291.
Parsons, K.M., Powell, E.N., Brett, C.E., Walker, S., Raymond, A., Callender, R., Staff, G., 1997. Shelf and Slope Experimental Taphonomy Initiative (SSETI): Bahamas and Gulf of Mexico. Proc. 8th Intl. Coral Reef Symposium, pp. 1807–1812.
Perry, C.T., Taylor, K.G., 2006. Inhibition of dissolution within shallow water carbonate sediments: impacts of terrigenous sediment input on syn-depositional carbonate diagenesis. Sedimentology 53, 495–513.
Powell, E.N., Parsons-Hubbard, K.M., Callender, W.R., Staff, G.M., Rowe, G.T., Brett, C.E., Walker, S.E., Raymond, A., Carlson, D.D., White, S., Heise, E.A., 2002. Taphonomy on the continental shelf and slope: two-year trends — Gulf of Mexico and Bahamas. Palaeogeography, Palaeoclimatology, Palaeoecology 184, 1–35.
Powell, E.N., Callender, W.R., Staff, G.M., Parsons-Hubbard, K.M., Brett, C.E., Walker, S.E., Raymond, A., Ashton-Alcox, K.A., 2008. Molluscan shell condition after eight years on the sea floor — taphonomy in the Gulf of Mexico and Bahamas. Journal of Shellfish Research 27, 191–225.
Powell, E.N., Staff, G.M., Callender, W.R., Ashton-Alcox, K.A., Brett, C.E., Parsons-Hubbard, K.M., Walker, S.E., Raymond, A., this issue. Taphonomic degradation of molluscan remains during thirteen years on the continental shelf and slope of the northwestern Gulf of Mexico. Palaeogeography, Palaeoclimatology, Palaeoecology doi:10.1016/j.palaeo.2010.12.006.
Rowe, G.T., Kennicutt, M.C., 2009. Northern Gulf of Mexico Continental Slope Habitats and Benthic Ecology Study — Final Report. U.S. Department of the Interior Minerals Management Service Gulf of Mexico OCS Region, New Orleans, p. 397.
Sanders, D., 2001. Burrow-mediated carbonate dissolution in rudist biostromes (Aurisina, Italy): implications for taphonomy in tropical, shallow subtidal carbonate environments. Palaeogeography, Palaeoclimatology, Palaeoecology 168, 39–74.
Sanders, D., 2003. Syndepositional dissolution of calcium carbonate in neritic carbonate environments: geological recognition, processes, potential significance. Journal of African Earth Sciences 36, 99–134.
Sassen, R., Joye, S., Sweet, S.T., DeFreitas, D.A., Milkov, A.V., MacDonald, I.R., 1999. Thermogenic gas hydrates and hydrocarbon gases in complex chemosynthetic communities, Gulf of Mexico continental slope. Organic Geochemistry 30, 485–497.
Smith, A.M., Nelson, C.S., 2003. Effects of early sea-floor processes on the taphonomy of temperate shelf skeletal carbonate deposits. Earth-Science Reviews 63, 1–31.
Soetaert, K., Hofmann, A.F., Middelburg, J.J., Meysman, F.J.R., Greenwood, J., 2007. The effect of biogeochemical processes on pH. Marine Chemistry 105, 30–51.
Stoessell, R.K., 1992. Effects of sulfate reduction on $CaCO_3$ dissolution and precipitation in mixing-zone fluids. Journal of Sedimentary Petrology 62, 873–880.
Ussler, I. Willliam, Paull, C.K., 2008. Rates of anaerobic oxidation of methane and authigenic carbonate mineralization in methane-rich deep-sea sediments inferred from models and geochemical profiles. Earth and Planetary Science Letters 266, 271–287.
Walker, S.E., Goldstein, S.T., 1999. Taphonomic tiering: experimental field taphonomy of molluscs and foraminifera above and below the sediment–water interface. Palaeogeography, Palaeoclimatology, Palaeoecology 149, 227–244.
Walter, L.M., Burton, E.A., 1990. Dissolution of recent platform carbonate sediments in marine pore fluids. American Journal of Science 290, 601–643.
Walter, L.M., Morse, J.W., 1984. Reactive surface area of skeletal carbonates during dissolution: effect of grain size. Journal of Sedimentary Petrology 54, 1081–1090.
Walter, L.M., Morse, J.W., 1985. The dissolution kinetics of shallow marine carbonates in seawater: a laboratory study. Geochimica et Cosmochimica Acta 49, 1503–1513.
Wang, W., Reimers, C.E., Wainright, S.C., Shahriari, M.R., Morris, M.J., 1999. Applying fiber-optic sensors for monitoring dissolved oxygen. Sea Technology 40, 69–74.